ACS OMEGA

http://pubs.acs.org/journal/acsodf

Article

Effect of Clay Minerals on Tensile Failure Characteristics of Shale

Fakai Dou, Peng Hou,* Zhirong Jia, Chunguang Wang, Hongbo Zhao, and Yanping Wang

Cite This: *ACS Omega* 2022, 7, 24219−24230

Read Online

ACCESS | Metrics & More | Article Recommendations

ABSTRACT: The effects of mass fraction, elastic modulus, and the spatial distribution of clay minerals on the failure behaviors of shale under the Brazilian disc split are investigated in this study based on a developed PFC^{2D} model. The feasibility of this established numerical model is validated by the load−displacement curves and fracture morphology of shale in the laboratory test. The influences of the mass fraction, elastic modulus, and spatial distribution of clay minerals on the tensile strength and failure behaviors of shale are comprehensively analyzed using the developed numerical model. The results show that the clay content has the strongest influence on the tensile strength of shale. The number of matrix cracks is sensitive to the clay distribution, and the complexity of the matrix fracture network in shale shows a positive correlation with the clay content. In addition, the variation of the clay modulus has a linear correlation with the macro elastic modulus of shale.

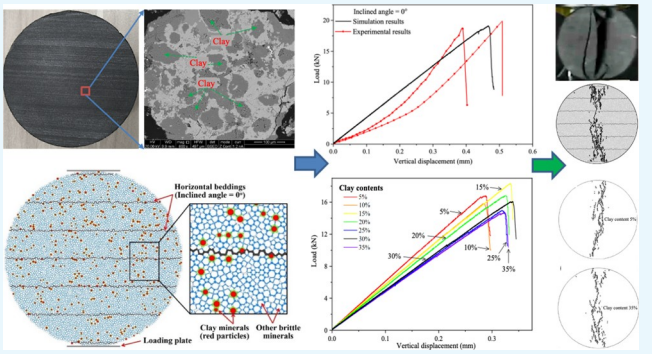

1. INTRODUCTION

The huge demand for clean energy has stimulated natural gas extraction and the corresponding engineering activities.[1,2] Taking shale gas extraction as an example, the effectiveness of hydraulic fracturing is closely related to the accurate knowledge of the formation mechanical properties.[3] Understanding the failure mechanism and failure process from the micro-level to the macro-level is a benefit to the unconventional gas/oil exploration and exploitation.[4] Therefore, the effects of shale's inherent heterogeneity on its mechanical properties and fracturing behaviors become hot issues in the field of hydraulic fracturing,[5,6] especially in recent years.

Tensile strength is a key parameter to judge crack initiation in hydraulic fracturing of shale reservoirs. Brazilian disc splitting test is an effective and usual method to obtain the indirect tensile strength of brittle material such as rocks and concretes. The tensile strength, the tensile strain distribution, and the crack initiation position[7] in Brazilian discs have aroused lots of attention. The early formula of splitting tensile strength assumes that the materials of Brazilian discs are homogeneous, isotropic, and linearly elastics before the brittle failure.[8,9]

$$\sigma_t = \frac{2P}{\pi Dt} \tag{1}$$

Regarding the rocks with layered structures, the transversely isotropic elastic theory is considered in the developed formula by[10] as follows

$$\sigma_t = \frac{2P}{\pi Dt}\left[(\sqrt[4]{E/E'})^{\cos(2\theta)} - \frac{\cos(4\theta)}{4}(b-1)\right] \tag{2}$$

The theoretical formula usually assumes that the rock materials are homogeneous. However, the shale gas reservoir includes complex mineral components. Up to now, the improvement of theoretical research is still not good at reflecting how the rock's inherent heterogeneity affects the crack propagation process. To some content, the numerical methods are competent to understand the effects of rock heterogeneity on the rock mechanical properties and fracture properties, which could also overcome the experimental uncertainly, especially from a micro-level.[11] Currently, numerical simulation studies on shale anisotropy mainly focus on the effect of weak bedding,[12−14] these studies have greatly deepened the understanding of the mechanical characteristics of shale anisotropy. For example, Wang et al.[15] found that the stratified rock discs showed obvious directionality in the tensile strength, which is manifested by the variation of strength with bedding orientation. Xia et al.[16] proposed that the combined effect of layered structure and flaws plays an important role in the crack propagation path and

Received: March 6, 2022
Accepted: June 22, 2022
Published: July 6, 2022

related failure patterns. As we know, the inherent anisotropy of shale is not only affected by the bedding properties but also the heterogeneity characteristics of mineral particles. The experimental test indicated that there are more than 10 mineral components detected in the Longmaxi shale formation.[12,17] Different mineral particles have different mechanical properties, which may affect the petrophysical properties of the shale reservoir. Wang et al.[18] investigated the relationships among composition, porosity, and permeability of Longmaxi shale and found that clay content is positively correlated with porosity and permeability. The previous studies indicated that the elastic modulus of quartz and dolomite is the highest, and that of clay including kaolinite and illite is the lowest, where the maximum difference value of their elastic modulus reaches 69 MPa.[19−21] Clay mineral is one of the important components in the shale matrix. Loucks and Ruppel[22] experimentally found that the average content of clay in the Barnett shale is 24.2%. Wu et al.[23] reported that the clay mineral content is less than 25% in the bottom of Longmaxi formation based on the information of composite log of shale lithofacies of well. Gao and Xiong[24] found that the clay content in Longmaxi Formation ranges from 20.6 to 64.3% by the field-emission scanning electron microscopy (FE-SEM) experiments. Sun et al.[25] found that the clay content of shale in Niutitang formation only ranges from 5.7 to 8.6%. Therefore, we can see that the clay mineral content of shale varies greatly under different geological conditions, and the influence of clay mineral on the mechanical characteristics of shale cannot be ignored. Current studies mainly reported that the clay content is closely related to the shale brittleness.[26,27] Guo et al.[28] verified that the shale gas formation with a high percentage of clay minerals exhibits a lower brittleness and prefers to generate the tabular fractures under hydraulic fracturing. However, the effects of clay mineral on the shale tensile strength and failure behaviors are rarely reported, which may cause some deviation in the prediction of fracture evolution in hydraulic fracturing of shale reservoirs.

The study aims to investigate the effects of clay heterogeneity inside shale on the mechanical properties and fracture morphology under indirect tensile conditions. First, a numerical model of the Brazilian disc split which considers the clay heterogeneity inside shale is developed by using particle flow code (PFC). Second, the simulation results of the established model were validated by comparing with the experimental results. Then, the effects of clay heterogeneity inside shale on the mechanical properties and fracture morphology under the Brazilian disc split were comparatively analyzed. The findings of this study are helpful to the accurate prediction of fracturing behaviors which could optimize the fracturing location, fracturing procedure, and economize the project cost of shale gas.

2. BRAZILIAN DISC SPLITTING MODEL

This study adopts a discrete element method to investigate the effects of clay minerals on the tensile failure characteristics of shale under Brazilian disc splitting. The reason why we chose PFC is that this method is competent to investigate the clay heterogeneity from the mineral particle level.

2.1. Geometric Model. The size and physical parameters of the established shale model are the same as the experimental specimens. Figure 1 shows the diagram of the established shale model. It is a two-dimensional intact disc of 50 mm in diameter, which is assembled by 7834 particles. It is assembled by 7834 particles and its porosity is 3%, which is within the

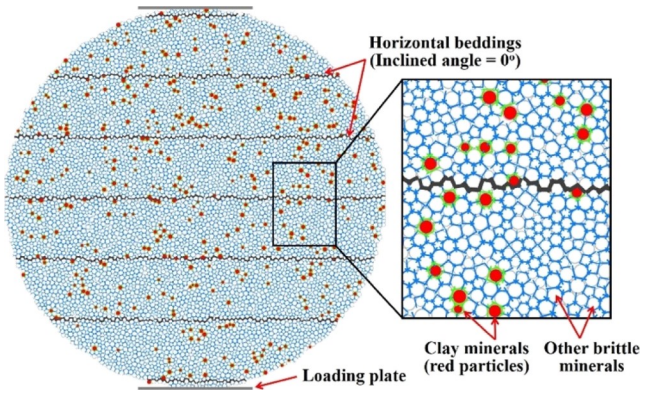

Figure 1. Brazilian disc model of shale in PFC^{2D} (clay content is 5%).

reasonable range of shale porosity.[18,29] The particle density is 2230 kg/m^3 and their diameters range from 0.4 to 0.7 mm. These particles in shale model have been divided in two parts. The red particles represent clay minerals while the white particles represent brittle minerals such as quartz and carbonate in the shale matrix. The green or blue lines around the particles mean the difference of strength parameters. The strength and elastic modulus of clay minerals should be smaller than other brittle minerals. Previous statistical results show that the spacing of bedding planes ranges from 0.2 to 0.8 mm.[30] However, it is difficult to set such tiny spacing of bedding planes in numerical models by considering the size effect. According to the modeling experience of PFC, the perpendicular distance between adjacent beddings is 10 times larger than the mean particle radius.[31] Thus, the perpendicular distance between adjacent beddings is set to 8 mm in the established shale model, which could avoid the size effects induced by dense beddings. The inclined angle is assumed as the angle between the horizontal line and the beddings. The variation of the inclined angle is only considered in the section of model verification. Because this study mainly focuses on the effects of shale heterogeneity induced by clay minerals, the inclined angle of beddings is set to 0° in the following sensitivity analysis.

2.2. Contact Model. The particles in the assembled model are connected by the built-in contact models, which controls the force−displacement relationship at the particle level. To distinguish the difference of mechanical properties between matrix and beddings, the matrix part of this established model adopts the parallel bond model (PBM, as shown in Figure 2), while the part of the beddings adopts the smooth joint model (SJM, as shown in Figure 3). The mechanical algorithm of PBM in PFC is developed by Potyondy and Cundall.[32] The

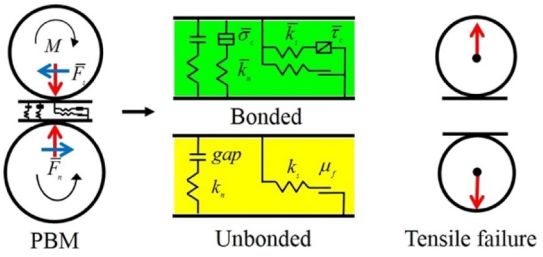

Figure 2. Motion and interaction of particles in the rock matrix (take the tensile failure as an example).

https://doi.org/10.1021/acsomega.2c01344
ACS Omega 2022, 7, 24219−24230

updating of contact forces in PFC follows the force−displacement relationship in Hooke's law.

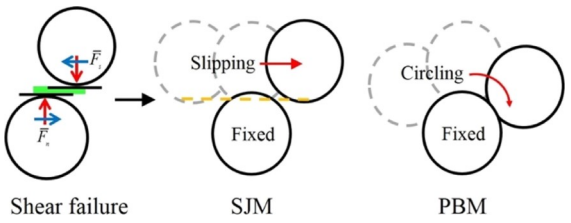

Figure 3. Particle motion in the matrix-bedding interface (take the shear failure as an example).

For the matrix part of the shale disc, the tensile stress $\bar{\sigma}$ of contacts is decided by the normal force $\bar{F}_n^{pb}$ and moment $\bar{M}^{pb}$, while the shear stress $\bar{\tau}$ is controlled by $\bar{F}_s^{pb}$. The cross-sectional area A and the inertia moment I is decided by the radius of particles in the established model. The default value of the moment-contribution factor β is 0.2. They are calculated by

$$\bar{\sigma} = \frac{\bar{F}_n^{pb}}{A} + \beta\frac{\bar{M}^{pb}\bar{R}}{I} \tag{3}$$

$$\bar{\tau} = \frac{\bar{F}_s^{pb}}{A} \tag{4}$$

Once the tensile or the shear stress of matrix contacts exceeds the presupposed strength parameters as shown in eq 5, the micro-crack (tensile or shear failure) will occur.

$$\bar{\sigma} > \bar{\sigma}_c^{pb}$$
$$\bar{\tau} > \bar{\tau}_c^{pb} \tag{5}$$

As shown in Figure 2, tensile failure means the detachment of parallel plates. Shear failure means the occurrence of a slip phenomenon between parallel plates. As shown in Figure 2, once the contact breaks, the contact state changes from bonded to un-bonded.

For the layered structures in shale discs, the application of SJM could better simulate the phenomenon that the particles of matrix parts slip along the presupposed weak structures (see in Figure 3). In addition, the dilatancy effect is also considered in SJM if the failure mode of contact belongs to shear failure. Before the occurrence of micro-cracks, the calculation of the normal force $\bar{F}_n^{sj}$ and shear force $\bar{F}_s^{sj}$ in SJM is similar to the PBM, which follows the force−displacement relationship in Hooke's law. Once the bonding of SJM is broken, the normal force in SJM with the dilatancy effect is updated as followed.[33,34]

$$\bar{F}_n^{sj} = \bar{F}_n^{sj} + \left(\frac{|\bar{F}_s^{sj}| - F_s^{\mu}}{\bar{k}_s^{sj}}\right)\cdot\bar{k}_n^{sj}\cdot\tan\varphi \tag{6}$$

$$\bar{F}_s^{\mu} = -\mu_f\bar{F}_n^{sj} \tag{7}$$

The calculation of contact stress in SJM does not consider the effects of moment in PBM. The calibrated microscopic parameters of PBM and SJM in Brazilian disc test model are listed in Table 1.

$$\bar{\sigma} = \frac{\bar{F}_n^{sj}}{A} \tag{8}$$

$$\bar{\tau} = \frac{\bar{F}_s^{sj}}{A} \tag{9}$$

Table 1. Micro Mechanical Parameters in the Validated Model of the Brazilian Disc Test

parameters (unit)	symbol	value
Young's modulus in PBM (GPa)	$\bar{E}_c$	0.105
stiffness ratio in PBM	$\bar{k}_n^{pb}/\bar{k}_s^{pb}$	1.5
particle friction coefficient	μ_{pb}	0.47
tensile strength in PBM (MPa)	$\bar{\sigma}_c^{pb}$	0.45
shear strength in PBM (MPa)	$\bar{\tau}_c^{pb}$	0.65
normal stiffness in SJM (GPa/m)	$\bar{k}_n^{sj}$	240.0
shear stiffness in SJM (GPa/m)	$\bar{k}_s^{sj}$	240.0
tensile strength in SJM (MPa)	$\bar{\sigma}_c^{sj}$	0.15
shear strength in SJM (MPa)	$\bar{\tau}_c^{sj}$	0.20
friction coefficient in SJM	μ_f	0.6
dilation angle in SJM (degree)	φ	20.0

3. MODEL VERIFICATION

3.1. Experimental Sample and Process. In this work, the established shale model of the Brazilian disc test is validated by laboratory test results. The shale samples were taken from the outcrop of Pengshui shale gas block which belongs to the Marine Silurian Longmaxi Formation shale in Southern China. The shale has a low clay mineral content of about 5%, and its average density is 2.23 g/cm^3. The shale reservoir is well developed and shows obvious bedding. The cylindrical samples with the size of Φ 50 mm × 25 mm were drilled in the direction parallel to the beddings of the shale, as shown in Figure 4a. There are considerable clay particles in the shale matrix microstructure (see Figure 4a). Brazilian splitting

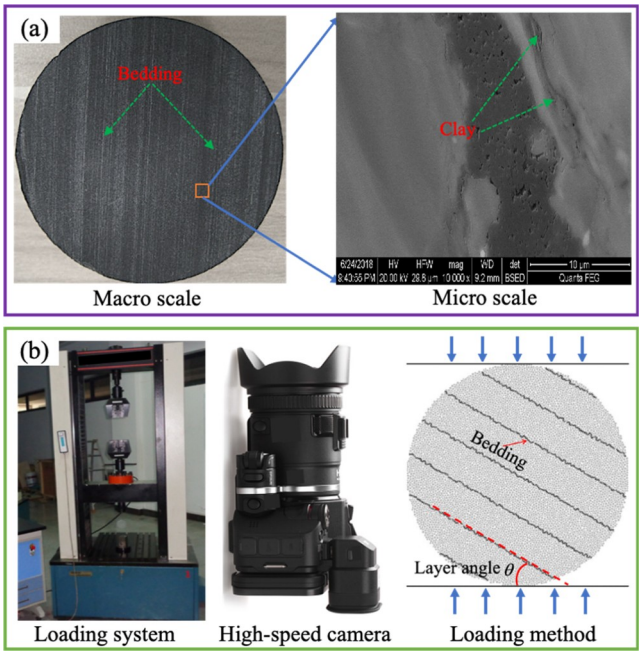

Figure 4. Shale specimen (a) and experimental system (b).

https://doi.org/10.1021/acsomega.2c01344
ACS Omega 2022, 7, 24219−24230

test was performed on CSS44100 electronic universal testing machine, as shown in Figure 4b. The maximum test force of the load machine is 100 kN. The loading process is controlled by the displacement and the rate is 0.1 mm/min. Meanwhile, the crack propagation process of the sample was recorded by a VC'S GC-PX100BAC high-speed camera with the highest shooting frequency of 500 fps. The loading method of the shale specimen is also shown in Figure 4b. In the laboratory test, five bedding inclined angles of 0, 30, 45, 60, and 90° were tested.

3.2. Comparison of Experimental and Numerical Results. Based on PFC, the common practice is to calibrate the micro-parameters of particles based on the macroscopic mechanical properties of the specimen.[35] As shown in Figure 5,

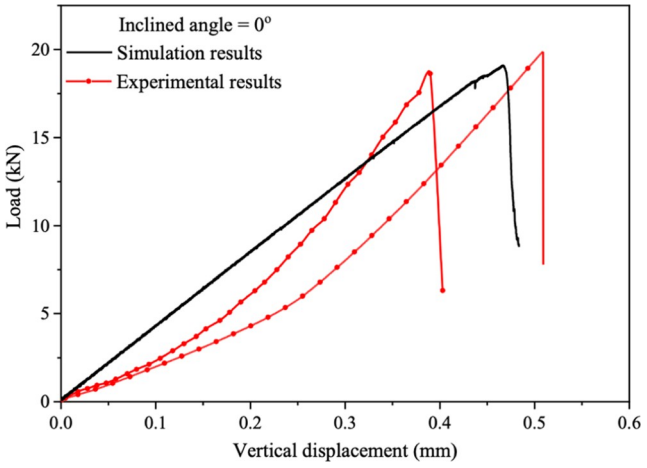

Figure 5. Comparison of the load−displacement curve at the bedding inclined angles of 0°.

the dotted line is obtained from the experimental result while the smooth line is obtained from the simulation result, where the bedding inclined angles of 0° is employed. The dotted line shows a concave trend in the initial loading stage and turns into a linear increase after the compaction stage. The compaction phenomenon is induced by the closure of the initial micro-cracks. Because the established shale model has finished the compaction stage before start loading, the load−displacement curve obtained from the numerical model directly shows a linear increase. By comparing the slope of the load−displacement curve in the elastic deformation stage and the peak load in Figure 5, it is found that the shape of load−displacement curve in the simulation result is similar to those in the laboratory tests.

Figure 6a−c shows three stages of crack evolution from the aspect of experimental results, numerical results, and Von Mises stress distribution, respectively. The load of initiation, propagation and failure stage is 95% (pre-peak stage), 75% (post-peak stage), and 20% (post-peak stage), respectively. The inclined angle of beddings is 0° under these circumstances. The black color in Figure 6b is used to reflect the matrix cracks. It shows that a small number of matrix cracks initiate from the location nearing the center and the loading position of the Brazilian disc at first. Then, a large number of matrix cracks propagate abruptly along the compressive diametral line and penetrate the Brazilian disc. There are also some micro-cracks occurring in beddings without gathering up. The Von Mises stress distribution in Figure 6c is presented by the sequence of the rainbow color in legends, which further reveals the evolution of rock's internal stress field. The mainstream view thought that the critical extension strain criterion could explain why the crack initiation position is located at the top and bottom locations, while the maximum tensile strength criterion is applied to explain why the crack initiation position is located at the center of the Brazilian discs.[36] Generally, the simulated crack propagation trajectory is similar to the experimental result. It indicates that the established shale model is competent to investigate the failure process of shale under the Brazilian disc test.

Figure 7 offers a contrastive analysis of the peak load between experimental and simulation results under different inclined angles. This is for the validation of the bedding strength parameters of the established shale model. The peak load marked by repeated trails shows a discreteness to some extent and their deviation from the mean value is less than 10%. The simulation results are within the range of fluctuation in most cases, which further validates the reliability of the established shale model.

4. SENSITIVITY ANALYSIS

Although shale is composed of a variety of minerals, the mechanical parameters of brittle minerals in shale are relatively close. Table 2 summarizes the elastic modulus of different minerals in shale according to the previous indentation tests. It can be seen that the mechanical properties of clay minerals are significantly weaker than those of brittle minerals. Therefore, this study mainly focuses on the effects of clay minerals on the tensile properties and fracture morphology of shale. The particles in the shale model are divided into two parts. One is the clay minerals; the other part refers to the brittle minerals. Table 3 lists the mechanical parameters of clay minerals and other brittle minerals applied in this shale model. The proportion relationship of elastic modulus in Table 3 refers to the related proportion relationship in Table 2. The effects of mass fraction, elastic modulus, and spatial distribution of clay minerals on the tensile properties and fracturing behaviors of shale are investigated in this chapter, respectively. This study mainly focuses on the effects of shale heterogeneity induced by matrix; thus, the inclined angle of beddings is set to 0° in the following sensitivity analysis.

4.1. Effects of Clay Content. According to the previous experimental results, the assumption of clay content ranges from 5 to 35% with an interval of 5% in this section. Figure 8 shows the distribution of clay minerals in shale discs, where the inclined angle of beddings is 0° and the same thing down here. The red particles in Figure 6 represent the clay minerals in shale discs. Figure 9 shows a series of simulated load−displacement curves under different clay contents. The peak load, the slope of the load−displacement curve, and the final vertical displacement are affected by the variation of clay contents.

The variation trend of peak load and the ratio of peak load to vertical displacement under different clay contents are further studied. As shown in Figure 10a, the mean value of peak load among all cases is 16.2 MPa and its standard deviation is 1.13 MPa. When the clay content is less than 20%, the simulated peak load is relatively higher than the mean value. The situation has changed if the clay content is larger than 20%. Generally, the peak load of the shale model shows a fluctuating downward trend with the increase in clay content. There is a positive correlation relationship between the ratio of

https://doi.org/10.1021/acsomega.2c01344
ACS Omega 2022, 7, 24219−24230

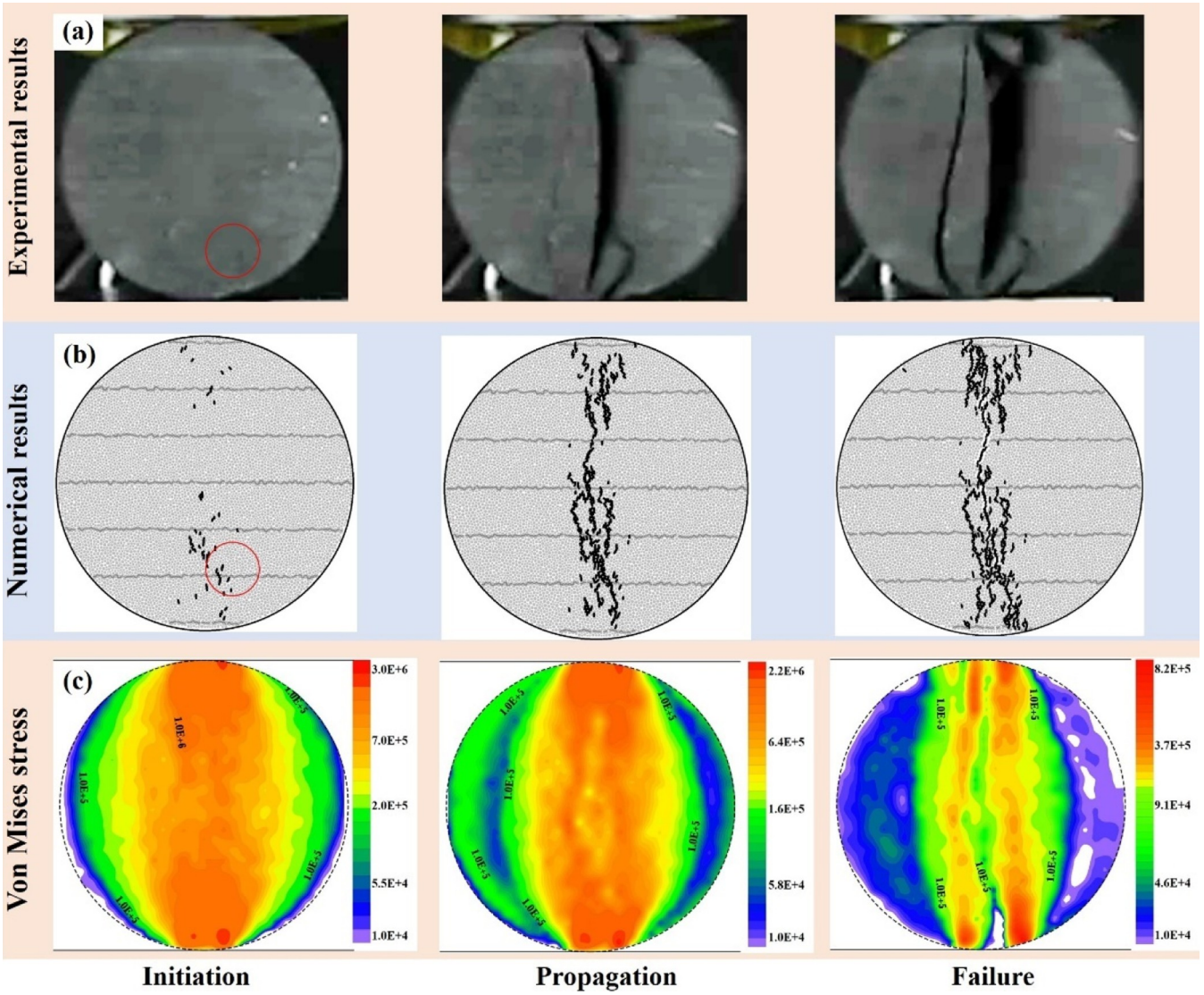

Figure 6. Comparison of the fracture propagation process between experimental (a) and numerical results (b) as well as the Von Mises stress distribution (c) at the bedding inclined angles of 0°.

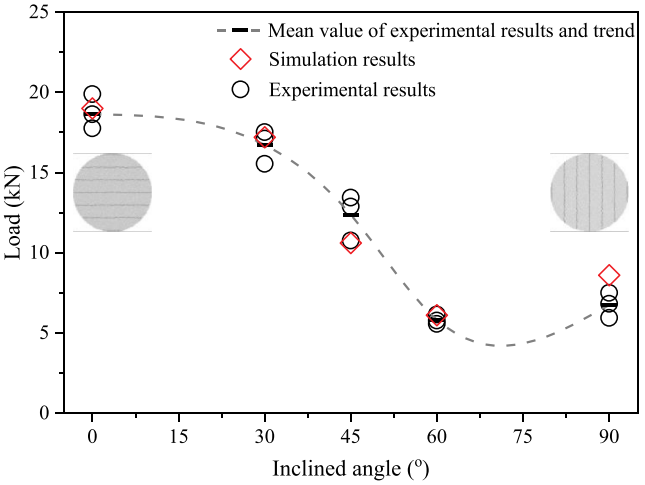

Figure 7. Variation trend of peak load between experimental and numerical results.

Table 2. Elastic Modulus of Different Minerals in Shale (GPa)

previous studies	quartz	carbonate	clay minerals
Shi et al.[19]	99	79	55−62
Liu and Wang[37]	86.25	72.4	24.12
Kumar et al.[21]	68−100	85−125	56−66

Table 3. Mechanical Parameters of Shale Matrix in the Established Model

parameters	other brittle minerals	clay minerals
elasticity modulus (GPa)	0.105	0.063
tensile strength (MPa)	0.45	0.27
shear strength (MPa)	0.65	0.39

peak load to vertical displacement and rock elastic modulus. Figure 10b shows the variation trend of the ratio of peak load to vertical displacement with the increase in clay contents. This ratio decreases from 59.2 to 45.8 as the clay content increases from 5 to 35%. It is more like a linear downward trend. This indicates that the rock macro elastic modulus decreases with

https://doi.org/10.1021/acsomega.2c01344
ACS Omega 2022, 7, 24219−24230

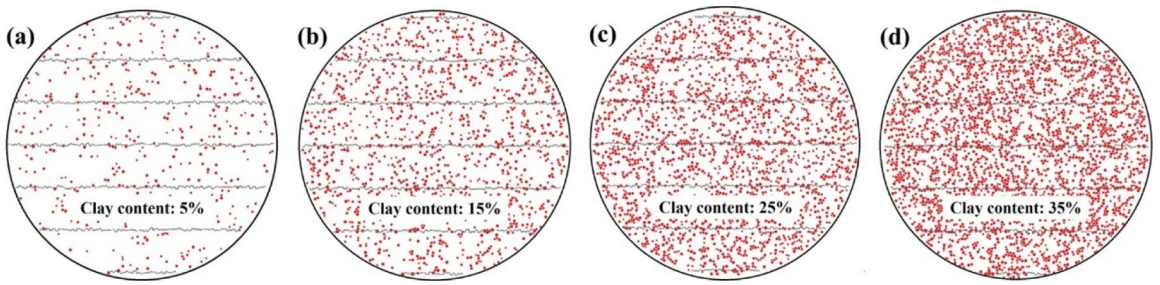

Figure 8. Distribution of clay minerals in shale discs under different clay contents [(a): clay content is 5%; (b): clay content is 15%; (c): clay content is 25%; and (d): clay content is 35%].

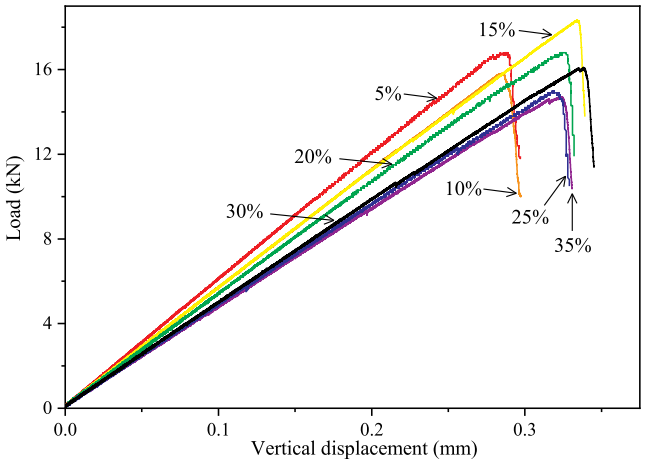

Figure 9. Comparison of load−displacement curves under different clay contents in the simulation of the Brazilian test.

the increase of the clay content. The fluctuation of the ratio of peak load to vertical displacement and especially the peak load may result from the variation of the spatial distribution of clay particles. We will further study this fluctuation in the Discussion section.

The effects of clay content on the matrix failures of shale discs are discussed in Figure 11. When the residual load decreases to 70% of the peak load, the number of matrix cracks is counted as a graph. In Figure 11a, the matrix tensile cracks are marked by blue blocks, while the matrix shear cracks are marked by white blocks. In this study, the number of matrix tensile cracks and matrix shear cracks are represented by Pbt and Pbs, respectively. There are about 19000 contacts in the established shale disc, most of the broken contacts result from tensile failure. The average values of total matrix tensile cracks (Pbt) and matrix shear cracks (Pbs) in Figure 11a are 322 and 79, while the corresponding standard deviation values are 31.2 and 16.5. Tensile failure is dominated under the Brazilian disc test, and it does not change by the variation of clay content. Here, the ratio of Pbt to Pbs (Pbt/Pbs) means the ratio of matrix tensile cracks to the matrix shear cracks, which is analyzed in Figure 11b. When the clay content ranges from 5 to 15%, the ratio of Pbt/Pbs linearly decreases from 7.4 to 3.4. When the clay content ranges from 15 to 35%, the downward trend disappears and the ratio of Pbt/Pbs is stable within a certain range. The clay content makes a difference in the failure mode of shale under the Brazilian disc test only if the mass fraction of clay minerals is less than 15%.

4.2. Effects on Elastic Modulus of Clay. The effects of the elastic modulus of clay minerals on the mechanical and failure behaviors can be investigated by adjusting the relative elastic modulus (the ratio of elastic modulus of clay to the other brittle minerals). In this section, the relative elastic modulus is set to 0.3, 0.4, 0.5, and 0.6 MPa, respectively. Additionally, the clay content in this numerical model is fixed at 35%. In Figure 12, there is no apparent variation in the shape of the load−displacement curve. While the slope of the load−displacement curve is getting smaller as the decrease of clay modulus. It implies that the micro elastic modulus of clay plays a role in the macro elastic modulus of shale rocks.

Figure 13 analyzed the effects of the micro elastic modulus of clay on the peak load and the ratio of peak load to vertical displacement, respectively. The simulation results in Figure

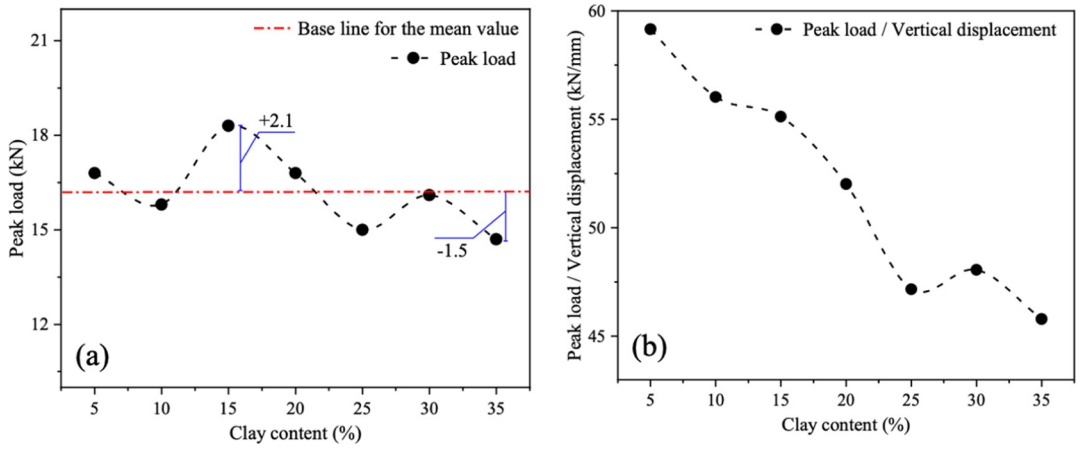

Figure 10. Effects of clay contents on the peak load (a) and the ratio of peak load to vertical displacement (b).

https://doi.org/10.1021/acsomega.2c01344
ACS Omega 2022, 7, 24219−24230

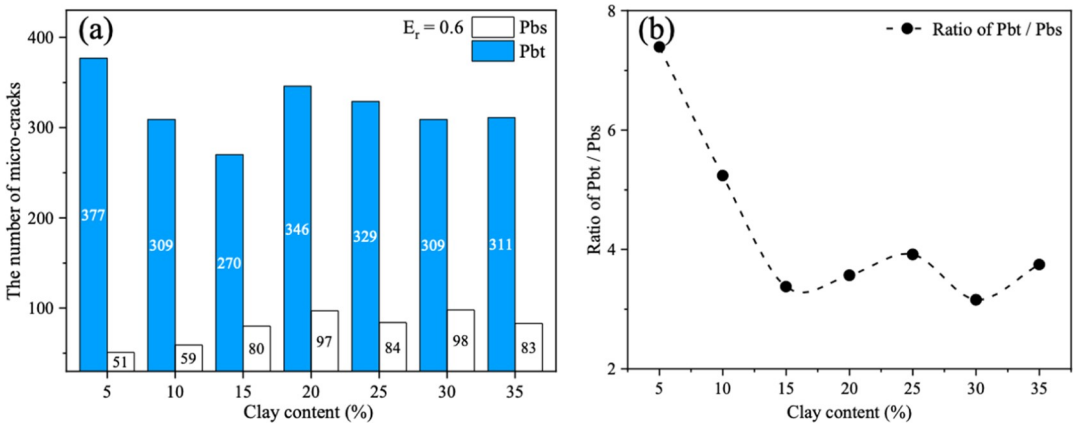

Figure 11. Effects of clay contents on the number of matrix-cracks (a) and failure mode (b) under Brazilian test.

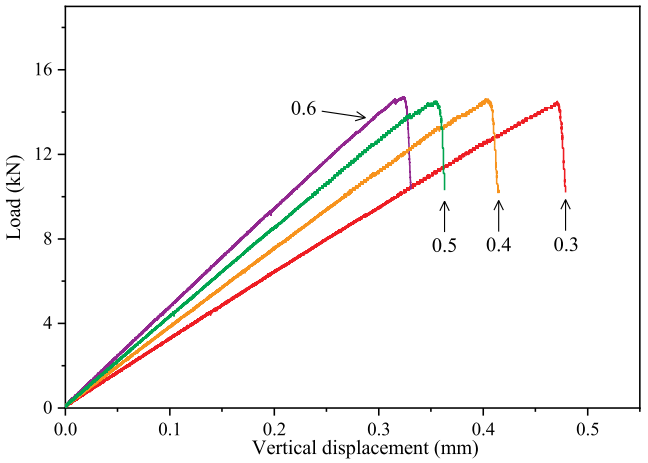

Figure 12. Comparison of load−displacement curves under different clay moduli in the simulation of the Brazilian test.

13a come from the circumstance that the mass fraction of clay minerals is 35%. Even under these conditions, the mean value of peak load among these cases is 14.6 MPa and its standard deviation is only 0.112 MPa. Under most circumstances, the proportion of clay minerals mainly ranges from 5% to 35%.[38,39] Thus, the micro elastic modulus of clay has a slight influence on the peak load. That is to say, the failure load of the shale disc is not sensitive to the variation of clay modulus. The clay modulus mainly affects the shale deformation rather than the failure load under the Brazilian disc tests. In contrast, the ratio of peak load to vertical displacement linearly increases from 30.6 to 45.8 as the clay elastic modulus increases from 0.3 to 0.6. The shale elastic modulus cannot be directly measured by the Brazilian disc test; however, the ratio of peak load to vertical displacement could be a reflection of shale elastic modulus. The simulation results in Figure 13b show that the micro elastic modulus of clay has a linear dependence relationship with the macro elastic modulus of shale rocks.

Figure 14 further investigated the effects of clay modulus on the total number of matrix cracks and the variation of failure mode under the Brazilian disc test, respectively. Due to the clay distribution and the proportion of clay minerals remaining the same in this section, the clay modulus is the unique variable. From Figure 14a, the number of matrix cracks varies little under different relative elastic modulus. The average values of total matrix tensile cracks and matrix shear cracks are 331 and 88, while the corresponding standard deviation values are 18.5 and 3.6. The fluctuation of total matrix cracks induced by clay modulus is insignificant. It indicates that the variation of clay modulus has limited influence on the rock damage degree. Similarly, in Figure 14b, the ratio of Pbt/Pbs hardly changes under different clay moduli. The average value of the ratio of Pbt/Pbs is 3.79, while the corresponding standard deviation value is 0.128. The variation of clay modulus has a positive impact on the rock elastic deformation; however, it has

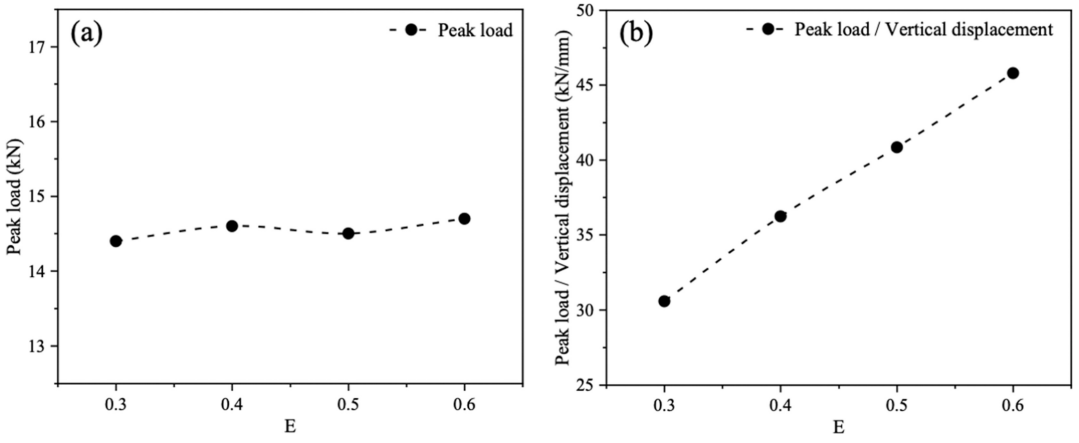

Figure 13. Effects of clay modulus on the peak load (a) and the ratio of peak load to vertical displacement (b).

https://doi.org/10.1021/acsomega.2c01344
ACS Omega 2022, 7, 24219−24230

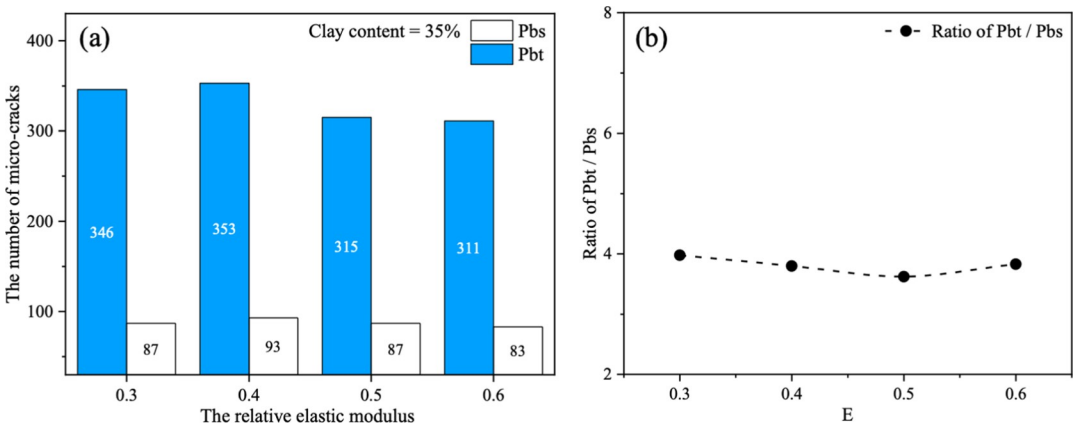

Figure 14. Effects of clay elastic modulus on the number of matrix-cracks (a) and failure mode (b) under Brazilian test.

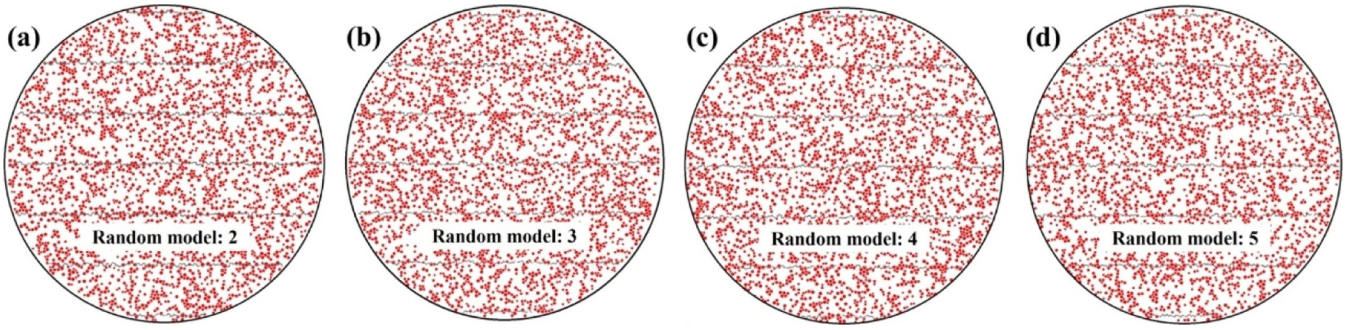

Figure 15. Distribution of clay minerals in shale discs under different random models [the clay content is 35%, (a): random model 2; (b): random model 3; (c): random model 4; and (d): random model 5].

a slight influence on the rock damage degree and the variation of failure mode.

4.3. Effects of Clay Distribution. There is a function called Random Number Generation in PFC. It can change the particle spatial distribution in the geometric model, while all the other parameters keep unchanged. In Section 4.3, the clay content is set to 35% and the relative elastic modulus is set to 0.6. Figure 15 shows the distribution of clay minerals in shale discs under the different random models. The particle size, the mechanical parameters of the contact model, and the loading conditions are the same among all cases. The clay distribution in Section 4.3 is the unique variable.

In the previous sections of this study, the random number usually defaults to 10001. To investigate the spatial distribution of clay minerals on the shale mechanical behaviors and failure behaviors under the Brazilian disc test, another four established models are conducted by adopting the random numbers 10002 (case 2), 10003 (case 3), 10004 (case 4), and 10005 (case 5), respectively. Under different clay distributions, the load−displacement curves are compared in Figure 16. The effects of clay distribution on the peak load, the slope of the load−displacement curves, and the failure mode of matrix-crack are further studied.

Figure 16 mainly reflects that the influences of clay distribution on the peak load and the ratio of peak load to vertical displacement. It mainly emphasizes the differences among five different clay distributions rather than variation trends. The effects of clay distribution on the peak load and the ratio of peak load to vertical displacement are shown in Figure 17. The horizontal axis in Figure 17 represents five independent cases. There is no progressive relationship

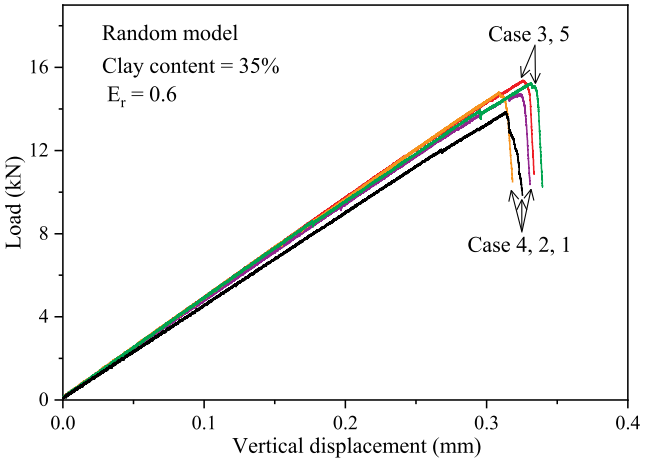

Figure 16. Comparison of load−displacement curves under different clay distributions in the simulation of the Brazilian test.

among them. In these five cases, the average value of peak load is 14.7 and its standard deviation is 0.64. By comparing Figures 17a and 13a of Section 4.2, the simulation results indicate that the clay distribution has a more obvious impact on the peak load than the clay modulus. In Figure 17b, the average value of the ratio of peak load to vertical displacement is 46.3 and its standard deviation value is 1.29, which indicates that the rock deformation is hardly affected by the clay distribution.

Figure 18a shows the total number of matrix cracks in shale discs by changing the spatial distribution of clay minerals. The average values of total matrix tensile cracks and matrix shear

https://doi.org/10.1021/acsomega.2c01344
ACS Omega 2022, 7, 24219−24230

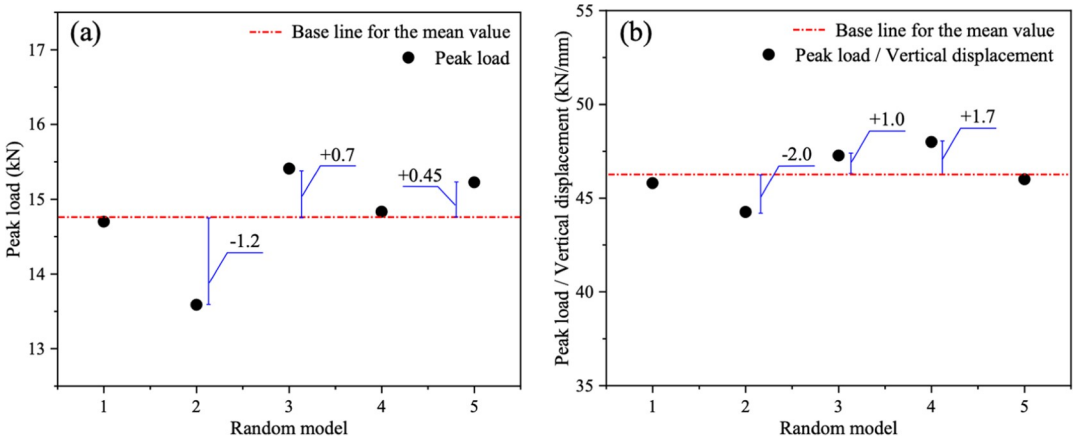

Figure 17. Effects of clay distribution on the peak load (a) and the ratio of peak load to vertical displacement (b).

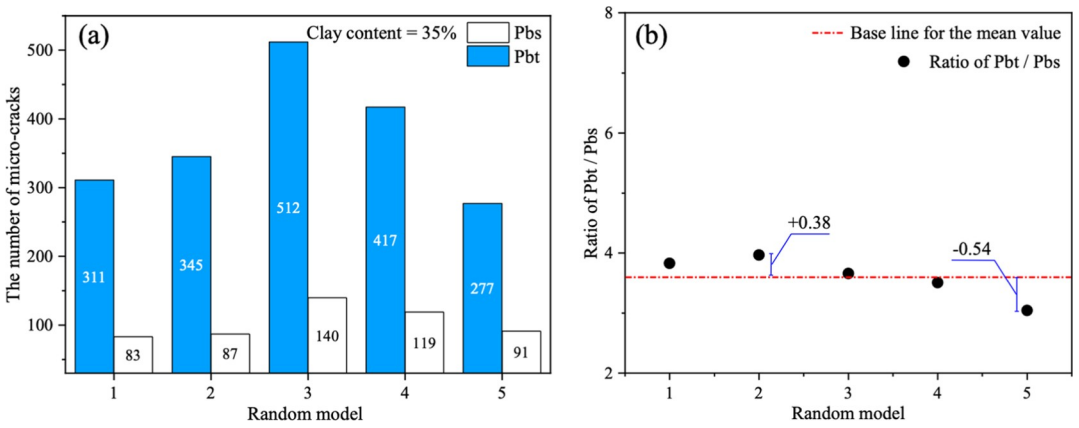

Figure 18. Effects of clay distribution on the number of matrix-cracks (a) and failure mode (b) under Brazilian test.

cracks are 372 and 104, while the corresponding standard deviation values are 83.8 and 22, respectively. Compared with the clay content and clay modulus, the total number of matrix cracks is more sensitive to the clay distribution. From Figure 18b, the average value of Pbt/Pbs under different clay distributions is 3.58 and its corresponding standard deviation value is only 0.31. That is to say, the spatial distribution of clay minerals could play a role in the number of matrix cracks; however, the failure mode of matrix crack is slightly affected.

5. DISCUSSION

The effects of clay content, clay modulus, and clay distribution on the mechanical and failure behavior of shale discs are analyzed in Section 4, respectively. In this part, the tensile strength and the fracture morphology of shale discs are comparatively analyzed under Brazilian disc tests. This section aims to find which factor plays a much more key role in tensile strength and fracture morphology.

5.1. Tensile Strength. By comparing three different sensitive factors, the simulation results of shale mechanical characteristics in Section 4 are further analyzed from the aspect of shale tensile strength. The shale tensile strength in Section 5 is calculated according to eq 1. Table 4 lists the average value, range, and standard deviation of shale tensile strength under different conditions. If the clay content in shale discs ranges from 5 to 35% with an interval of 5%, the range and the standard deviation of tensile strength are 1.83 MPa and 0.58 MPa. While if the relative modulus of clay minerals ranges from 0.3 to 0.6 with an interval of 0.1, its range and related standard deviation of tensile strength are 0.15 MPa and 0.06 MPa. That is to say, the variation of clay content has a more significant effect on the shale tensile strength than the variation of clay modulus. Under the same clay contents and the micro-mechanical parameters, the fluctuation of tensile strength is also affected by the spatial distribution of clay minerals. The range and the standard deviation of shale tensile strength induced by clay distribution are 0.93 and 0.32 MPa. Among these three factors, the effects of clay content on the shale tensile strength are much more significant than the clay distribution and clay modulus. Usually, the clay content in shale gas reservoirs is less than 35% and the range of the relative modulus of clay minerals is smaller than 0.3. Therefore, the effects of clay modulus on the variation of shale tensile strength are so little as to be unnoticeable.

Table 4. Tensile Strength of the Shale Sample after the Brazilian Disc Test (Unit: MPa)

clay parameters	average	range	standard deviation
clay content	8.26	1.83	0.58
clay modulus	7.41	0.15	0.06
clay distribution	7.51	0.93	0.32

5.2. Fracture Morphology. The simulation results of shale fracture morphology under different sensitive factors are further analyzed from the aspect of fractal dimension. The complexity of fracture morphology is mainly decided by the

https://doi.org/10.1021/acsomega.2c01344
ACS Omega 2022, 7, 24219−24230

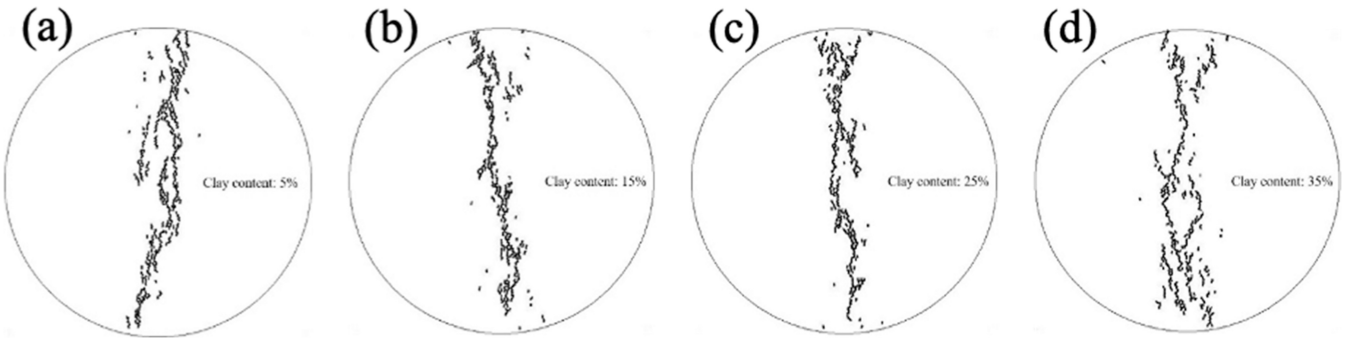

Figure 19. Pictures of shale matrix cracks before binarization treatment [take the models of clay contents as example. (a): clay content is 5%; (b): clay content is 15%; (c): clay content is 25%; and (d): clay content is 35%].

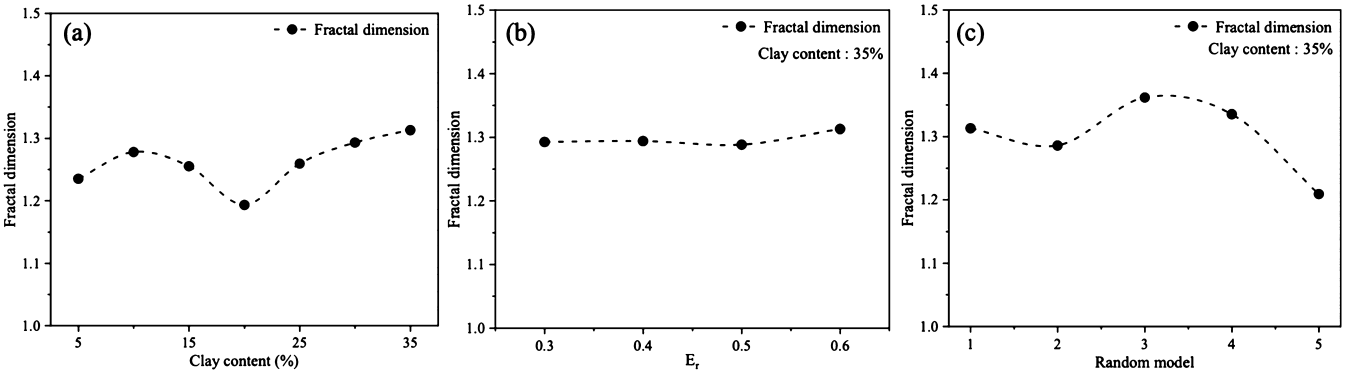

Figure 20. Variation of fracture fractal dimension under different sensitive factors [(a) the clay content, (b) the relative modulus, and (c) the clay distribution].

matrix cracks.[34] Based on the simulation results under different clay contents, clay modulus, and clay distributions, this part mainly discusses which sensitive factors play a much more key role in the complexity of fracture morphology under the same loading conditions. Taking the models of clay contents as an example, Figure 19 shows the final fracture morphology under different clay contents. The short black lines represent matrix cracks.

This study adopts the box-counting procedure to calculate the fractal dimension of final fracture morphology. During the calculation process, the pictures of shale matrix cracks will be fully covered by 2^n square boxes (n ranges from 1 to 9 with an interval of 1), the number of square boxes containing matrix cracks is $M(n)$. When lg $M(n)$ and n lg 2 are projected in an orthogonal logarithmic coordinate system, the slope represents the fractal dimension of matrix cracks D.[40] The detailed calculation formula is expressed below.

$$D = \lim_{n\to\infty} \frac{\lg M(n)}{n \lg 2} \tag{10}$$

The simulated final fracture morphology of the shale disc such as the pictures in Figure 19 is used to measure the fractal dimension by using the box-counting procedure in MATLAB. The variation trend of fracture fractal dimension under different clay contents, the relative modulus, and the clay distribution are counted in Figure 18. As shown in Figure 20a, the fractal dimension of the matrix cracks shows a slow and fluctuating upward trend with the increase of clay content. When the clay content is 20%, the related fractal dimension shows a significant fall. The variation of the clay content will cause the redistribution of clay minerals. While Figure 20c shows that the redistribution of clay minerals may also cause the fluctuation of fracture fractal dimension. That is to say, the fluctuation of fractal dimension in Figure 20a may result from the redistribution of clay minerals. Comparatively, the effects of the relative modulus of clay minerals on the fracture fractal dimension are unnoticeable (In Figure 20b).

Table 5 lists the average, range and standard deviation of fracture fractal dimension under different circumstances. The range and the standard deviation of fractal dimension induced by clay distribution are 0.1525 and 0.0523, which is larger than the corresponding data of clay content and clay modulus. The range and the standard deviation of fractal dimension induced by clay modulus are only 0.0248 and 0.0095, respectively. It indicates that the variation of clay modulus plays an insignificant role in the complexity of fracture morphology. Additionally, the effect of clay content on the fracture fractal dimension is much more obvious than clay modulus. However, these influences are also affected by the clay distribution.

Table 5. Fractal Dimension of Matrix Fracture Morphology after BST (Unit: 1)

clay parameters	average	range	standard deviation
clay content	1.2610	0.1199	0.0365
clay modulus	1.2971	0.0248	0.0095
clay distribution	1.3010	0.1525	0.0523

6. CONCLUSIONS

This study developed a PFC2^D model of shale Brazilian disc test by considering the effects of inherent shale heterogeneity. The effects of the clay content, clay modulus, and the clay

https://doi.org/10.1021/acsomega.2c01344
ACS Omega 2022, 7, 24219−24230

distribution on the shale mechanical and fracturing behaviors were comparatively studied through the developed shale model. The main conclusions of this investigation are summarized below:

(1) Among the factors of the clay content, clay modulus, and the clay distribution, the clay content has the strongest influences on the shale failure load and tensile strength, followed by clay distribution, and the variation of clay modulus has the lowest influences on it.

(2) The ratio of peak load to vertical displacement means the load required for a unit displacement of the indenter, which reflects shale elastic modulus. This ratio shows a fluctuating downward trend with the increase of clay content and a linearly upward trend with the increase of clay modulus. It indicated that the mass fraction and elastic modulus of clay minerals could significantly affect the shale failure load and deformation degree.

(3) The dominated failure mode will not be changed by the variation of clay content, clay modulus, and clay distribution. Comparatively, the total number of matrix cracks is more sensitive to the spatial distribution of clay minerals.

(4) The complexity of the matrix fracture network could be quantitatively characterized by fractal dimension. The fractal dimension of matrix cracks shows a slow and fluctuating upward trend as the increase of clay content, and this fluctuation of variation trend is closely related to the spatial distribution of clay minerals.

AUTHOR INFORMATION

Corresponding Author

Peng Hou − *IPPH, Purdue University, West Lafayette, Indiana 47907, United States;* orcid.org/0000-0002-2752-3958; Email: phou1989@163.com, hou119@purdue.edu

Authors

Fakai Dou − *School of Civil and Architectural Engineering, Shandong University of Technology, Zibo 255000, China*

Zhirong Jia − *School of Civil and Architectural Engineering, Shandong University of Technology, Zibo 255000, China*

Chunguang Wang − *School of Civil and Architectural Engineering, Shandong University of Technology, Zibo 255000, China*

Hongbo Zhao − *School of Civil and Architectural Engineering, Shandong University of Technology, Zibo 255000, China*

Yanping Wang − *School of Civil and Architectural Engineering, Shandong University of Technology, Zibo 255000, China*

Complete contact information is available at: https://pubs.acs.org/10.1021/acsomega.2c01344

Notes

The authors declare no competing financial interest.

ACKNOWLEDGMENTS

The authors are grateful for the financial support from the Shandong Provincial Natural Science Foundation (ZR2020ME269 and ZR2021MD011) and the Start-up funding for doctoral research at Shandong University of Technology in 2021 (no. 421068).

ABBREVIATIONS

FE-SEM, field-emission scanning electron microscopy; PFC, particle flow code; PBM, parallel bond model; SJM, smooth joint model

REFERENCES

(1) Hou, P.; Liang, X.; Gao, F.; Dong, J. B.; He, J.; Xue, Y. Quantitative visualization and characteristics of gas flow in 3D pore-fracture system of tight rock based on Lattice Boltzmann simulation. *J. Nat. Gas Sci. Eng.* **2021**, *89*, 103867.

(2) Hou, P.; Su, S. J.; Liang, X.; Gao, F.; Cai, C. Z.; Yang, Y. G.; Zhang, Z. Z. Effect of liquid nitrogen freeze-thaw cycle on fracture toughness and release rate of saturated sandstone. *Eng. Fract. Mech.* **2021**, *258*, 108066.

(3) Liang, X.; Hou, P.; Xue, Y.; Yang, X. Y.; Gao, F.; Liu, J. A fractal perspective on fracture initiation and propagation of reservoir rocks under water and nitrogen fracturing. *Fractals* **2021**, *29*, 2150189.

(4) Zhang, Y.; Zhang, Z.; Sarmadivaleh, M.; Lebedev, M.; Barifcani, A.; Yu, H.; Iglauer, S. Micro-scale fracturing mechanisms in coal induced by adsorption of supercritical CO_2. *Int. J. Coal Geol.* **2017**, *175*, 40−50.

(5) Hou, P.; Chen, G.; Su, S.; Yang, Y.; Cai, C.; Wang, S.; Qiu, J.; Gao, F. Influence of various control factors on fracture toughness and fracture energy of sandstone subjected to liquid nitrogen cooling. *Energy Fuels* **2022**, *36*, 397.

(6) Hou, P.; Xue, Y.; Gao, F.; Dou, F. K.; Su, S. J.; Cai, C. Z.; Zhu, C. H. Effect of liquid nitrogen cooling on mechanical characteristics and fracture morphology of layer coal under Brazilian splitting test. *Int. J. Rock Mech. Min.* **2022**, *151*, 105026.

(7) Liang, X.; Hou, P.; Yang, X. J.; Xue, Y.; Teng, T.; Gao, F.; Liu, J. On estimating plastic zones and propagation angles for mixed mode I/II cracks considering fractal effect. *Fractals* **2022**, *30*, 2250011.

(8) Mellor, M.; Hawkes, I. Measurement of Tensile Strength by Diametral Compression of Discs and Annuli. *Eng. Geol.* **1971**, *5*, 173−225.

(9) Hou, P.; Su, S. J.; Gao, F.; Liang, X.; Wang, S. C.; Gao, Y. A.; Cai, C. Z. Influence of Liquid Nitrogen Cooling State on Mechanical Properties and Fracture Characteristics of Coal. *Rock Mech. Rock Eng.* **2022**, *55*, 3817−3836.

(10) Claesson, J.; Bohloli, B. Brazilian test: stress field and tensile strength of anisotropic rocks using an analytical solution. *Int. J. Rock Mech. Min.* **2002**, *39*, 991−1004.

(11) Zhang, Y.; Zhang, Z. K.; Arif, M.; Lebedev, M.; Busch, A.; Sarmadivaleh, M.; Iglauer, S. Carbonate rock mechanical response to CO_2 flooding evaluated by a combined X-ray computed tomography - DEM method. *J. Nat. Gas Sci. Eng.* **2020**, *84*, 103675.

(12) Chong, Z.; Li, X.; Hou, P.; Wu, Y.; Zhang, J.; Chen, T.; Liang, S. Numerical Investigation of Bedding Plane Parameters of Transversely Isotropic Shale. *Rock Mech. Rock Eng.* **2017**, *50*, 1183−1204.

(13) Yang, S.-Q.; Yin, P.-F.; Huang, Y.-H. Experiment and Discrete Element Modelling on Strength, Deformation and Failure Behaviour of Shale Under Brazilian Compression. *Rock Mech. Rock Eng.* **2019**, *52*, 4339−4359.

(14) Wang, J.; Wang, Y.; Yang, L.; Chang, T. Q.; Jiang, Q. P. Effects of Bedding Geometry and Cementation Strength on Shale Tensile Strength Based on Discrete Element Method. *Shock Vib.* **2021**, *2021*, 7805617.

(15) Wang, P.; Cai, M.; Ren, F. Anisotropy and directionality of tensile behaviours of a jointed rock mass subjected to numerical Brazilian tests. *Tunn. Undergr. Space Technol.* **2018**, *73*, 139−153.

(16) Xia, K.; Ren, R.; Liu, F. Numerical analysis of mechanical behavior of stratified rocks containing a single flaw by utilizing the particle flow code. *Eng. Anal. Bound. Elem.* **2022**, *137*, 91−104.

(17) Hou, P.; Gao, F.; Yang, Y.; Zhang, X.; Zhang, Z. Effect of the layer orientation on mechanics and energy evolution characteristics of shales under uniaxial loading. *Int. J. Min. Sci. Technol.* **2016**, *26*, 857−862.

(18) Wang, Q.; Wang, T.; Liu, W.; Zhang, J.; Feng, Q.; Lu, H.; Peng, P. A. Relationships among composition, porosity and permeability of Longmaxi Shale reservoir in the Weiyuan Block, Sichuan Basin, China. *Mar. Pet. Geol.* **2019**, *102*, 33−47.
(19) Shi, X.; Jiang, S.; Lu, S. F.; He, Z. L.; Li, D. J.; Wang, Z. X.; Xiao, D. S. Identification of mechanical properties of Longmaxi shale with beddings by nanoindentation tests: A case study on Silurian Longmaxi Formation of Youyang area in southeast Chongqing. *Pet. Explor. Dev.* **2019**, *46*, 155−164.
(20) Shukla, P.; Kumar, V.; Curtis, M.; Sondergeld, C. H.; Rai, C. S. Nanoindentation studies on shales *In 47th US Rock Mechanics/Geomechanics Symposium*; US Rock Mechanics Association: San Francisco, CA, USA, 2013.
(21) Kumar, V.; Curtis, M. E.; Gupta, N. *Estimation of elastic properties of organic matter in Woodford shale through nano-indentation measurements*; SPE, 2012; p 162778.
(22) Loucks, R. G.; Ruppel, S. C. Mississippian Barnett Shale: Lithofacies and depositional setting of a deep-water shale-gas succession in the Fort Worth Basin, Texas. *AAPG Bull.* **2007**, *91*, 579−601.
(23) Wu, L.; Hu, D.; Lu, Y.; Liu, R.; Liu, X.; Liu, X. F. Advantageous shale lithofacies of Wufeng Formation-Longmaxi Formation in Fuling gas field of Sichuan Basin, SW China. *Pet. Explor. Dev.* **2016**, *43*, 208−217.
(24) Gao, Z. Y.; Xiong, S. L. Methane Adsorption Capacity Reduction Process of Water-Bearing Shale Samples and Its Influencing Factors: One Example of Silurian Longmaxi Formation Shale from the Southern Sichuan Basin in China. *J. Earth Sci.* **2021**, *32*, 946−959.
(25) Sun, W.; Zuo, Y.; Wu, Z.; Liu, H.; Zheng, L.; Shui, Y.; Xi, S.; Lou, Y.; Luo, X. The distribution characteristics of brittle minerals in the Lower Cambrian Niutitang Formation in northern Guizhou. *J. Nat. Gas Sci. Eng.* **2021**, *86*, 103752.
(26) Liu, Z.; Sun, Z. New brittleness indexes and their application in shale/clay gas reservoir prediction. *Pet. Explor. Dev.* **2015**, *42*, 129−137.
(27) Gong, F.; Zeng, L. B.; Di, B. R.; Wei, J. X.; Ding, P. B.; Liu, C. N.; Li, H. Experimental investigation of clay content on brittleness of synthetic shale. *In 79th EAGE Conference and Exhibition*; EarthDoc: Paris, France, 2017.
(28) Guo, T.; Zhang, S.; Ge, H.; Wang, X.; Lei, X.; Xiao, B. A new method for evaluation of fracture network formation capacity of rock. *Fuel* **2015**, *140*, 778−787.
(29) Cao, T.; Xu, H.; Liu, G. X.; Deng, M.; Cao, Q. G.; Yu, Y. Factors influencing microstructure and porosity in shales of the Wufeng-Longmaxi formations in northwestern Guizhou, China. *J. Pet. Sci. Eng.* **2020**, *191*, 107181.
(30) Chong, Z.; Li, X.; Hou, P. Experimental and Numerical Study of the Effects of Layer Orientation on the Mechanical Behavior of Shale. *Arabian J. Sci. Eng.* **2019**, *44*, 4725−4743.
(31) Dou, F.; Wang, J. G.; Zhang, X.; Wang, H. Effect of joint parameters on fracturing behavior of shale in notched three-point-bending test based on discrete element model. *Eng. Fract. Mech.* **2019**, *205*, 40−56.
(32) Potyondy, D. O.; Cundall, P. A. A bonded-particle model for rock. *Int. J. Rock Mech. Min.* **2004**, *41*, 1329−1364.
(33) Dou, F.; Wang, J.; Leung, C. The Impacts of Bedding Strength Parameters on the Micro-Cracking Morphology in Laminated Shale under Uniaxial Compression. *Appl. Sci.* **2020**, *10*, 5496.
(34) Dou, F.; Wang, J. G.; Leung, C. F.; Ma, Z. The alterations of critical pore water pressure and micro-cracking morphology with near-wellbore fractures in hydraulic fracturing of shale reservoirs. *Eng. Fract. Mech.* **2021**, *242*, 107481.
(35) Yang, S.-Q.; Huang, Y.-H.; Jing, H.-W.; Liu, X.-R. Discrete element modeling on fracture coalescence behavior of red sandstone containing two unparallel fissures under uniaxial compression. *Eng. Geol.* **2014**, *178*, 28−48.
(36) Li, D.; Wong, L. N. Y. The Brazilian Disc Test for Rock Mechanics Applications: Review and New Insights. *Rock Mech. Rock Eng.* **2013**, *46*, 269−287.
(37) Liu, W. N.; Wang, M. Research on evaluation of shale reservoir brittleness based on differences in the rock mechanical characteristics. *Contemp. Chem. Ind.* **2020**, *49*, 458−461.
(38) Hu, W.; Guo, Y. T.; Wang, L.; Hou, Z. K.; Xu, F. An experimental study on mechanical anisotropy of shale reservoirs at different depths. *Rock Soil Mech.* **2017**, *38*, 2496−2506.
(39) Guo, W.; Shen, W.; Li, X.; Wang, N.; Liu, X.; Zhang, X.; Zhou, S. Study on mechanical characteristics and damage mechanism of the Longmaxi Formation shale in southern Sichuan Basin, China. *Energy Explor. Exploit.* **2020**, *38*, 454−472.
(40) Zhou, M.; Zhang, Y.; Zhou, R.; Hao, J.; Yang, J. Mechanical Property Measurements and Fracture Propagation Analysis of Longmaxi Shale by Micro-CT Uniaxial Compression. *Energies* **2018**, *11*, 1409.

https://doi.org/10.1021/acsomega.2c01344
ACS Omega 2022, 7, 24219−24230